Electron removal from molecular hydrogen by fully stripped ions at intermediate energies

L. Meng, C. O. Reinhold, and R. E. Olson
Department of Physics and Laboratory for Atomic and Molecular Research, University of Missouri–Rolla, Rolla, Missouri 65401-0249
(Received 19 May 1989)

A classical phase-space model of the hydrogen molecule is presented and applied to the study of the electron-capture and -ionization processes in collisions of fully stripped ions with H_2 at intermediate impact energies and charge states from 1 to 10. The model is based on the independent-electron and the impact-parameter approximations. The electron–impinging-ion and electron–target-nuclei interactions are exactly taken into account. The interaction between the electrons is approximated by model potentials. The calculated total cross sections for production of free electrons and capture of one electron are in good agreement with different experimental data. The ratio between the capture cross sections from molecular and atomic hydrogen targets is also analyzed and compared with available empirical scalings. It is found that this ratio varies from a value less than 1 at low impact energy to 4 at higher energies. The reasons for these differences are discussed. A comparison is made between the capture cross sections for different orientations of the hydrogen molecule.

I. INTRODUCTION

The theoretical study of the electron-capture and -ionization processes in collisions of ions with atoms has been the object of several works in recent decades. The first models that appeared in the literature were successfully developed for ion-atom collisions at either high or low impact velocities; i.e., either $v_p/v_e \gg 1$ or $v_p/v_e \ll 1$, v_p and v_e being the velocity of the projectile and the electron in its initial state, respectively. However, only a few approximations[1–5] have been successful in predicting cross sections in agreement with the experiments in the intermediate impact energy or velocity region (i.e., $v_p \simeq v_e$). Some of the most important reasons for the failure of the low- and high-energy approximations in this energy range are (i) both the ionization and capture channels contribute significantly to the electron-removal cross sections, and the correlation between these channels cannot be neglected; and (ii) neither the interaction between the projectile and the active electron nor that between the active electron and target core can be considered as perturbations during the collision.[6,7]

Several rigorous theoretical models satisfying these conditions are available now to study the electron-capture and -ionization processes in ion-atom collisions at intermediate energies, and could, in principle, be easily generalized to treat ion-molecule collisions at intermediate energies. However, due to the large computational effort that the calculations would involve, no complete work has been performed yet in this energy range even for the simplest neutral molecule (i.e., H_2). In contrast, several experimental measurements are available in this energy range for collisions of multiply charged ions with H_2.

To our knowledge, the most successful calculations performed in the intermediate energy range for ion-H_2 collisions that can be found in the literature are the molecular-orbital expansion of Kimura, Chapman, and Lane[8] (low-to-intermediate energies) and the unitarized-close-coupling model of Shingal and Lin[9] (intermediate-to-high energies). Previous but not so successful calculations in the same energy range were performed by Sural and Sil[10] and Sidis and de Bruijn[11] who used a small expansion of the electronic wave function in atomic orbitals along with roughly approximated matrix elements.

In this work we present the first classical trajectory Monte Carlo (CTMC) model for the treatment of collisions of multiply charged ions with H_2 targets. The CTMC technique is well known for its application in ion-atom collisions in the intermediate-to-high velocity range.[1,2] The main hypothesis of the CTMC technique is that the state of the collision system can be represented by a real phase-space probability density which obeys the classical Liouville equation of motion[12] and which initially resembles the quantum-mechanical position and momentum probability densities. For completely stripped ions colliding with hydrogenlike atoms no other hypothesis is assumed; i.e., all the interactions are exactly taken into account and all the possible final partitions of the system are included in the model simultaneously.

More than one-electron systems are generally studied by assuming that the interactions between the electrons can be approximated by central screened Coulomb[13] or model potential[14–16] interactions. In the present model for ion-H_2 collisions, outlined in Sec. II, this approximation is also applied. However, the electron–impinging-ion and electron–target-nuclei interactions are exactly taken into account. Two-electron CTMC models including the interaction between the electrons have also appeared in the literature during the last years for He targets.[17,18] However, these models are not completely developed yet.

In Sec. III, we compare our calculated total cross sections for capture of one electron and production of free electrons with several experimental data for collisions of multiply charged ions with H_2. The charge state of the projectiles varies from 1 to 10 and the impact energy range under consideration is 10 keV/amu–1 MeV/amu.

In Sec. III we also analyze the differences between the cross sections for atomic and molecular hydrogen targets. In the first estimations of the electron-removal cross sections from H_2, it was assumed that the hydrogen molecule could be considered as two free H atoms and, consequently, the cross sections for H_2 could be approximated by twice the cross sections for H. However, as has been demonstrated experimentally,[19,20] this hypothesis is only valid (within an uncertainty of 20%) for the ionization process at intermediate-to-high impact energies. Our calculations confirm the experimental findings and allow us to explain some of the reasons for the differences between the capture cross sections from H and H_2 targets.

Finally, we also include in Sec. III a discussion about the contribution of the different orientations of the H_2 molecule to the averaged capture cross section over all the molecular orientations. This kind of study is of interest, since experimental investigations on this subject are in progress.[21] Atomic units will be used throughout the following text.

II. THEORY

The classical trajectory Monte Carlo technique for ion-atom collisions has been completely described by previous authors.[1,2,16] In brief, this technique consists of three consecutive steps: (i) sampling the initial projectile-target configurations, (ii) numerical integration of the equations of motion, and (iii) final test of reactions and calculation of cross sections. In this work we have developed a generalization of these steps to ion-H_2 collisions as presented in the following subsections.

As in previous theoretical works on ion-H_2 collisions at intermediate energies,[9,22] the following hypotheses will be assumed.

(i) The straight-line impact-parameter approximation,[23] i.e, the movement of the target nuclei, will be neglected during the collision time and the trajectory of the projectile will be approximated by $\mathbf{b}+\mathbf{v}_p t$, where $\mathbf{b}$ is the impact parameter and $\mathbf{v}_p$ is the impact velocity.

(ii) The independent-electron approximation,[24] i.e., the interaction between the electrons will be approximated by static model potentials.

A. Initial conditions

Consider the collision system of Fig. 1 in which an impinging ion (P) collides with a hydrogen molecule composed of two electrons (1 and 2) and two nuclei (A and B). The origin of the coordinate system is located at the center of mass of A and B, which is supposed to remain at rest. The experimental value of 1.402 a.u. is assigned to the distance R_{H_2} between the target nuclei.

The initial conditions for the system can be divided into the initial conditions for the projectile and those for the target. The initial conditions for the projectile are

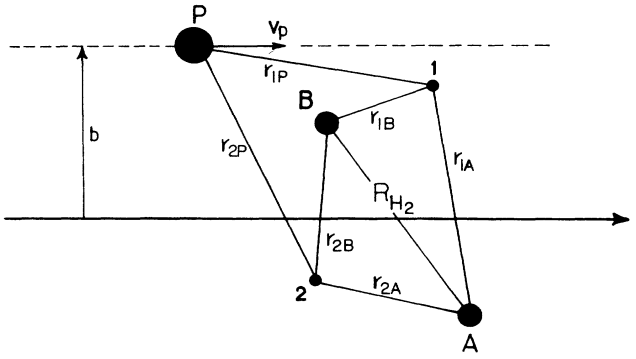

FIG. 1. Coordinate system in ion-H_2 collisions. A and B, H_2 nuclei; P, projectile; 1 and 2, electrons.

specified by its distance to the center of mass of the target, its velocity, and the impact parameter $\mathbf{b}$. The initial distance needs to be chosen large enough so that the interaction between the projectile and the electrons can be neglected at the beginning of the collision. The impact parameter is chosen so as to provide a uniform flux of incident particles. Denoting by b,ϕ_b the polar components of $\mathbf{b}$, this is done by generating ϕ_b and b^2 uniformly in the intervals $[0,2\pi]$ and $[0,b^2_{\max}]$, where $b_{\max}$ is an impact parameter above which the ionization or capture processes are negligible.

The initial conditions for the target are specified by the orientation of the molecule and the initial electronic configuration. First, the initial electronic conditions are generated for a fixed orientation (along the z axis) of the molecule. Then, the positions and momenta of the electrons and the nuclei are rotated randomly in three Euler angles ϕ, θ, and ψ so as to reproduce a homogeneous spherical distribution of the orientation of the molecule. As demonstrated by Abrines and Percival;[1] this can be done by generating uniformly $\cos\theta$, ϕ, and ψ in the intervals

$$\cos\theta\in[-1,1],\quad \phi,\psi\in[0,2\pi]\ . \tag{1}$$

For a fixed orientation of the molecule along the z axis, the electronic initial positions and momenta are sampled from the following initial two-electron phase-space distribution:

$$f_i(\mathbf{r}_1,\mathbf{r}_2,\mathbf{p}_1,\mathbf{p}_2)=\tfrac{1}{2}[f_\alpha(\mathbf{r}_1,\mathbf{p}_1)f_\beta(\mathbf{r}_2,\mathbf{p}_2) +f_\beta(\mathbf{r}_1,\mathbf{p}_1)f_\alpha(\mathbf{r}_2,\mathbf{p}_2)]\ , \tag{2}$$

where

$$f_{\alpha,\beta}(\mathbf{r},\mathbf{p})=k\delta\left[\frac{\mathbf{p}^2}{2}-\frac{1}{r_A}-\frac{1}{r_B}+V_{\alpha,\beta}(\mathbf{r})-E_i\right]\ , \tag{3}$$

k is a normalization constant, and $E_i=-0.567$ a.u. denotes the experimental ionization potential of H_2 (Ref. 25), which is obtained from a transition between $v=0$ states. Our two-electron distribution $f_i(\mathbf{r}_1,\mathbf{r}_2,\mathbf{p}_1,\mathbf{p}_2)$ is constructed in terms of two one-electron microcanonical distributions $f_{\alpha,\beta}(\mathbf{r},\mathbf{p})$, which describes those situations in which one electron is more probably found around the

nucleus A or B, respectively. The model potentials $V_{\alpha,\beta}$ represent the mean interaction between the electrons and depend on the initial configurations. In order to calculate these potentials, we appeal to the quantum-mechanical wave function for the ground state of H_2 as calculated by Wang[26]

$$\psi = c[\phi(r_{1A})\phi(r_{2B}) + \phi(r_{1B})\phi(r_{2A})] , \tag{4}$$

where

$$\phi(r) = \frac{\lambda^{3/2}}{\sqrt{\pi}} e^{-\lambda r} , \tag{5}$$

c is a normalization constant, and λ takes a value of 1.166, which is obtained by a variational calculation of the total energy. According to Weinbaum,[27] this approximated wave function represents the major part of more elaborated wave functions.

The model potential is then calculated as

$$V_{\alpha,\beta}(\mathbf{r}) = \left\langle \phi(r'_{B,A}) \left| \frac{1}{|\mathbf{r}-\mathbf{r}'|} \right| \phi(r'_{B,A}) \right\rangle = \frac{1}{r_{B,A}} [1 - (1+\lambda r_{B,A}) e^{-2\lambda r_{B,A}}] . \tag{6}$$

Therefore, in either of the distributions f_α or f_β, the electron interacts with a core H_2^+ through a potential $W_{\alpha,\beta}(\mathbf{r}) = -1/r_A - 1/r_B + V_{\alpha,\beta}(\mathbf{r})$, which satisfies the following asymptotic behaviors:

$$W_{\alpha,\beta} \underset{r\to\infty}{\sim} -\frac{1}{r} ,$$
$$W_{\alpha,\beta} \underset{r_A\to 0}{\sim} -\frac{1}{r_A} , \tag{7}$$
$$W_{\alpha,\beta} \underset{r_B\to 0}{\sim} -\frac{1}{r_B} .$$

In order to justify the use of our initial distribution given by expression (2), we compare in Figs. 2 and 3 the resulting classical one-electron probability densities

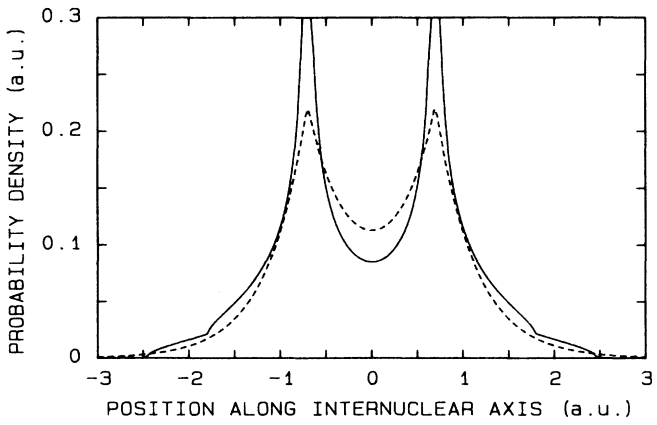

FIG. 2. One-electron probability density of the position along the internuclear axis of H_2. Solid line, present work; dashed line, quantum-mechanical distribution obtained from Wang's wave function (Ref. 26).

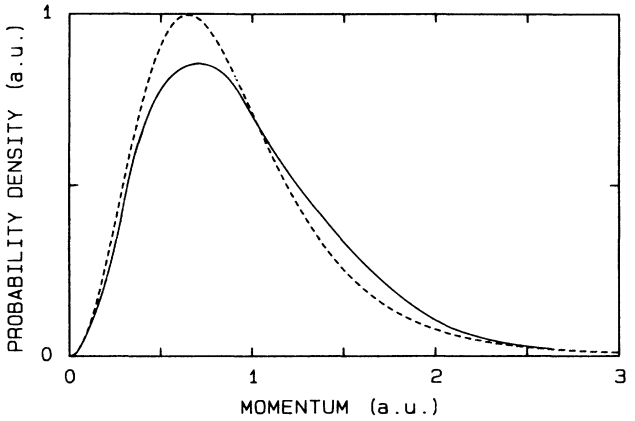

FIG. 3. One-electron probability density of the modulus of the momentum of H_2. Solid line, present work; dashed line, quantum-mechanical distribution obtained from Wang's wave function (Ref. 26).

$P^{\mathrm{CM}}(\mathbf{r}_1)$ and $P^{\mathrm{CM}}(\mathbf{p}_1)$ with the corresponding one-electron quantum-mechanical ones obtained from Wang's wave function (4), $P^{\mathrm{QM}}(\mathbf{r}_1)$ and $P^{\mathrm{QM}}(\mathbf{p}_1)$. These distributions can be calculated as

$$P^{\mathrm{CM}}(\mathbf{r}_1) = \int d\mathbf{r}_2 d\mathbf{p}_1 d\mathbf{p}_2 f_i(\mathbf{r}_1,\mathbf{r}_2,\mathbf{p}_1,\mathbf{p}_2) , \tag{8}$$

$$P^{\mathrm{CM}}(\mathbf{p}_1) = \int d\mathbf{r}_1 d\mathbf{r}_2 d\mathbf{p}_2 f_i(\mathbf{r}_1,\mathbf{r}_2,\mathbf{p}_1,\mathbf{p}_2) , \tag{9}$$

$$P^{\mathrm{QM}}(\mathbf{r}_1) = \int d\mathbf{r}_2 |\psi(\mathbf{r}_1,\mathbf{r}_2)|^2 , \tag{10}$$

$$P^{\mathrm{QM}}(\mathbf{p}_1) = \int d\mathbf{p}_2 |\tilde{\psi}(\mathbf{p}_1,\mathbf{p}_2)|^2 , \tag{11}$$

where

$$\tilde{\psi}(\mathbf{p}_1,\mathbf{p}_2) = \frac{1}{(2\pi)^3} \int d\mathbf{r}_1 d\mathbf{r}_2 e^{i(\mathbf{p}_1\cdot\mathbf{r}_1 + \mathbf{p}_2\cdot\mathbf{r}_2)} \psi(\mathbf{r}_1,\mathbf{r}_2) .$$

Figures 2 and 3 show that the classical distributions resemble to some extent the quantum-mechanical ones. We would like to note that even though the expression of our two-electron distribution looks like the expression of Wang's wave function and the distributions in the figures are similar, the one-electron distributions resulting from $f_{\alpha,\beta}$ differ from the corresponding one-electron distributions resulting from $\phi(r_{A,B})$. While the latter are one-center distributions, the former are two-center distributions. This introduces ionic terms in our model, as is favored by Weinbaum.

In order to calculate the cross sections, only one of the terms of the initial two-electron distribution needs to be considered. For example, the initial conditions for electrons 1 and 2 can always be sampled from f_α and f_β, respectively. Fortunately, a method to sample initial conditions from two-center initial distributions like $f_{\alpha,\beta}$ has been already developed in a previous work.[16] The last part of this section is devoted to this method. For simplicity, we will use the same notation $W(r_A,r_B)$ to denote both potentials $W_{\alpha,\beta} = -1/r_A - 1/r_B + V_{\alpha,\beta}(\mathbf{r})$.

Suppose that the initial state of an electron with Cartesian phase-space coordinates $\mathbf{r}=(x,y,z)$, $\mathbf{p}=(p_x,p_y,p_z)$ is given by

$$F(\mathbf{r},\mathbf{p})=k\delta[E_i-\mathbf{p}^2/2-W(r_A,r_B)] , \tag{12}$$

where k is a normalization constant. In order to sample initial conditions from this distribution, we perform the transformation

$$(\mathbf{r},\mathbf{p})\rightarrow(E,\xi,\eta,\phi_r,\nu_p,\phi_p) , \tag{13}$$

defined by

$$\xi=\frac{2}{R_{H_2}}(r_A+r_B),\quad \eta=\frac{2}{R_{H_2}}(r_A-r_B) ,$$
$$\phi_r=\tan^{-1}(y/x) , \tag{14}$$

and

$$\nu_p=\frac{p_z}{p},\quad \phi_p=\tan^{-1}(p_y/p_x) ,$$
$$E=\frac{p^2}{2}+W(r_A,r_B) , \tag{15}$$

where ξ, η, and ϕ_r denote the elliptical coordinates and $\theta_p=\cos^{-1}\nu_p$, and ϕ_p are the spherical angles of the momentum. The new variables are confined to the intervals

$$E\in(-\infty,0),\quad \xi\in[1,\infty],\quad \eta\in[-1,1] ,$$
$$\nu_p\in[-1,1],\quad \phi_p,\phi_r\in[0,2\pi] , \tag{16}$$

and the constraint

$$\frac{\mathbf{p}^2}{2}=E_i-W(\xi,\eta)>0 . \tag{17}$$

The Jacobian of this transformation is

$$J=\left[\frac{R_{H_2}}{2}\right]^3(\xi^2-\eta^2)\{2[E-W(\xi,\eta)]\}^{1/2} . \tag{18}$$

Therefore the probability density in terms of the new coordinates becomes

$$F(E,\xi,\eta,\phi_r,\nu_p,\phi_p)=k\delta(E-E_i)\left[\frac{R_{H_2}}{2}\right]^3(\xi^2-\eta^2)$$
$$\times\{2[E_i-W(\xi,\eta)]\}^{1/2} . \tag{19}$$

Since this form of the probability distribution does not depend on the variables ϕ_r, ν_p, and ϕ_p, it is concluded that these variables are uniformly distributed in the intervals given above. For the variables ξ and η, a different procedure is used. Integrating Eq. (19) over E, ϕ_r, ν_p, and ϕ_p, we obtain the probability density of these variables,

$$\rho(\xi,\eta)=\begin{cases}k'(\xi^2-\eta^2)[E_i-W(\xi,\eta)]^{1/2} & \text{if } E_i>W(\xi,\eta) ,\\ 0 & \text{if } E_i\le W(\xi,\eta) .\end{cases} \tag{20}$$

In order to sample initial values of η and ξ from this distribution a usual procedure, such as that described by Cohen,[28] can be used. Suppose that ξ_{max} is a value of ξ above which the constraint (17) is not satisfied for any value of η and that ρ_{max} is an upper bound of $\rho(\xi,\eta)$. Then the procedure is as follows. First, three values ξ, η, and χ are selected randomly and uniformly in the intervals $(0,\xi_{max})$, $(-1,1)$, and $(0,\rho_{max})$, respectively. Then $\rho(\xi,\eta)$ is evaluated and compared with χ. If $\rho(\xi,\eta)>\chi$, the selected values for ξ and η are accepted. Otherwise, new values of ξ, η, and χ are randomly selected and the process is repeated.

B. Dynamics

If the initial conditions for electrons 1 and 2 are, respectively, sampled from f_α and f_β, the electronic Hamiltonian can be written as

$$H=\frac{\mathbf{p}_1^2}{2}+\frac{\mathbf{p}_2^2}{2}-\frac{q}{r_{1P}}-\frac{q}{r_{2P}}$$
$$+W_\alpha(r_{1A},r_{1B})+W_\beta(r_{2A},r_{2B}) , \tag{21}$$

where q denotes the charge of the fully stripped impact ion. For a given set of initial conditions, the dynamics of the system is determined by numerically integrating the Hamilton equations:

$$\dot{\mathbf{p}}_i=-\frac{\partial H}{\partial \mathbf{r}_i},\quad \dot{\mathbf{r}}_i=\frac{\partial H}{\partial \mathbf{p}_i},\quad i=1,2 . \tag{22}$$

C. Reaction channels and cross sections

Under the restrictions of the present model, the possible reaction channels are

$$A^{q+}+H_2\rightarrow\begin{cases}A^{q+}+H_2^{++}+e^- & \text{(single ionization)}\\ A^{q+}+2H^++2e^- & \text{(double ionization)}\\ A^{(q-1)+}+H_2^+ & \text{(single capture)}\\ A^{(q-2)+}+2H^+ & \text{(double capture)}\\ A^{(q-1)+}+2H^++e^- & \text{(transfer ionization)}\\ A^{q+}+H_2^* & \text{(elastic and excitation) .}\end{cases} \tag{23}$$

The cross sections for these processes are obtained by examining the final binding energies of each of the electrons referred to the projectile and the target nuclei. If, for example, these energies indicate that both electrons are neither bound to nuclei nor to the projectile, then the corresponding counter for the double-ionization process is increased by 1.

Suppose that N_δ is the total number of successful final-state test that are obtained for channel δ after sampling N initial target-projectile configurations. Then the total cross section for this channel is given by

$$\sigma_\delta=\frac{N_\delta}{N}\pi b_{max}^2 . \tag{24}$$

In order to directly compare with experiments, we will present in this work the cross sections for production of free electrons σ_- and capture of one electron $\sigma_{q,q-1}$. The cross section $\sigma_{q,q-1}$ is obtained by addition of the cross sections for single capture σ_{SC} and transfer ionization σ_{TI}:

$$\sigma_{q,q-1}=\sigma_{SC}+\sigma_{TI} . \quad (25)$$

The cross section for production of free electrons is obtained in terms of the cross sections for single ionization σ_{SI}, transfer ionization σ_{TI}, and double ionization σ_{DI}. Since the experimental data for production of free electrons are obtained by measuring the ejected electrons, the cross section for double ionization is counted twice. Therefore

$$\sigma_{-}=\sigma_{SI}+\sigma_{TI}+2\sigma_{DI} . \quad (26)$$

We would like to note that in a previous article the contribution of the double ionization was incorrectly considered only once.[16] Since the double ionization for incident protons is negligible in comparison with the single ionization, the results obtained by these authors are correct. However, we have observed that the correct addition of the double ionization is crucial when the projectile charge is increased.

In a recent article Wetmore and Olson[29] observed that a certain fraction of the double-capture cross section calculated by means of independent-electron models has to be added to the transfer-ionization cross section. This is due to the fact that, in a double-capture reaction, both electrons often finish in excited states of the projectile. If the interaction between the electrons were explicitly taken into account, these kind of reactions would lead to autoionization of the projectile. In this article we have performed calculations with and without the corrections due to autoionization after double-electron capture. We have estimated these corrections by means of recent calculations of the capture cross sections to different final n levels in collisions of multiply charged ions with atomic hydrogen.[30,31] We have concluded that for H^+ and He^{2+} projectiles, about 10% and 80% of the double-capture cross section should be added to the transfer-ionization cross section, respectively. For projectile charges above 3, almost all the double-capture cross section should be considered to be part of the transfer-ionization cross section. As we will show in the following section, the double-capture followed by autoionization makes a major contribution to the total cross sections at low impact energies, while at high impact energies it is negligible.

III. RESULTS AND DISCUSSION

In Fig. 4 we display the results of our CTMC calculations of the total cross section for production of free electrons with and without the consideration of the autoionizing double capture in collisions of multiply charged ions with molecular hydrogen. These cross sections are compared with different experimental data. Since there are no available data for incident C^{6+} and O^{8+} ions, we include in the figure the empirical predictions of the nondissociative ionization cross section of Ref. 32. From the figure, it can be clearly seen that the autoionizing double capture plays a very important role at low impact energies, and its contribution improves considerably the agreement with the experiments. In general, a fairly good agreement can be observed between theory and experiment, except in the upper part of the impact energy range considered. There, it is well known that while the classical ionization cross sections behave as $1/v_p^2$, the correct high-energy limit is given by the first Born approximation as $(C+\ln v_p)/v_p^2$.

In Fig. 5 we display the free-electron production cross section as a function of the charge state q of the projectile at two different collision energies. The q^2 scaling given by the first Born approximation is also plotted as a reference. This figure shows that our calculations at 100 keV/amu predict a large departure from this scaling, in agreement with the experiments. This departure is greater if the autoionizing double capture is not included, in agreement with the calculations of Ref. 32. At 500 keV/amu, the dependence of the cross sections on projectile charge approaches the q^2 scaling, as expected.

In Fig. 6 we compare our cross section for capture of one electron $\sigma_{q,q-1}$ in collisions of multiply charged ions with molecular hydrogen with several different experimental data. A very good agreement can be observed between theory and experiment except for incident protons at low collision energies. As in the case of collisions of protons with atomic hydrogen, CTMC is unable to describe the quasiresonant mechanism that dominates the

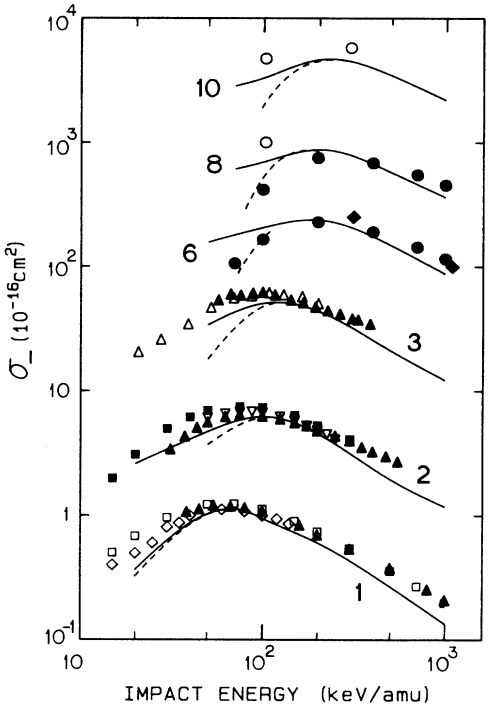

FIG. 4. Free-electron production cross section σ_- in $A^{q+}+H_2$ collisions. The data in the figure are numbered by the value of the projectile charge and are scaled as $A^+\times 0.5$, $A^{2+}\times 1$, $A^{3+}\times 5$, $A^{6+}\times 10$, $A^{8+}\times 25$, and $A^{10+}\times 100$. Solid and dashed curves, present work with and without autoionization modifications. ●, empirical prediction of Janev, Phaneuf, and Hunter (Ref. 32) for nondissociative ionization. Experimental data ◇, de Heer, Schutten, and Moustafa (Ref. 33); □ and ■, Rudd *et al.* (Refs. 34 and 35); ▲ and △, Shah and Gilbody (Ref. 20); ▽, Puckett, Taylor, and Martin (Ref. 36); ◆, Schlachter *et al.* (Ref. 37); ○, Berkner *et al.* (Ref. 38).

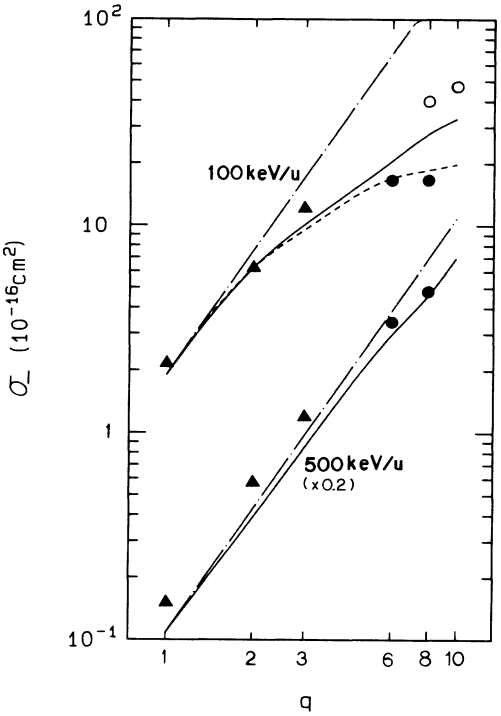

FIG. 5. Free-electron production cross section as a function of the charge state of the impact ion in $A^{q+}+H_2$ collisions. Solid and dashed curves represent cross sections with or without autoionization modifications, respectively. Dotted-dashed lines represent the behavior that a q^2 scaling would give. The symbols are experimental data interpolated from Fig. 4.

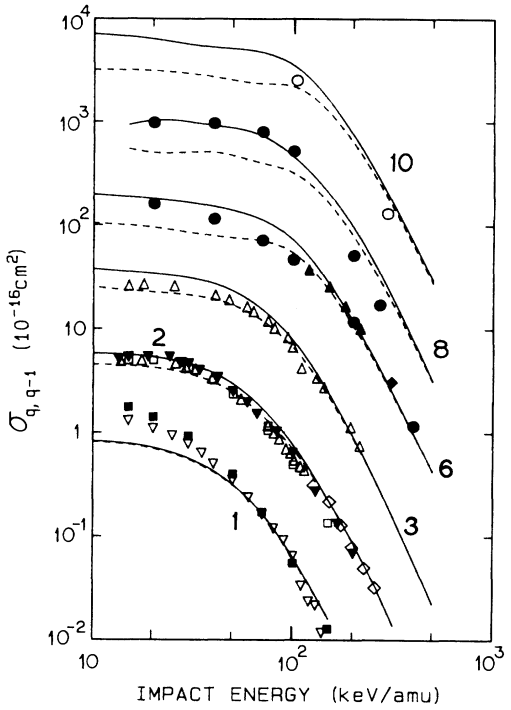

FIG. 6. One-electron capture cross section $\sigma_{q,q-1}$ in $A^{q+}+H_2$ collisions. The data in the figure are numbered by the value of the projectile charge and are scaled as $A^{+}\times 0.2$, $A^{2+}\times 5$, $A^{3+}\times 2$, $A^{6+}\times 5$, $A^{8+}\times 20$, and $A^{10+}\times 100$. Solid and dashed curves, present work with and without autoionization modifications, respectively. ●, Janev, Phaneuf, and Hunter (Ref. 32); experimental data, ■ and □, Rudd *et al.* (Refs. 34 and 35); ▽, de Heer, Schutten, and Moustafa (Ref. 33); ▽, Olson *et al.* (Ref. 39); △, Shah and Gilbody (Refs. 40 and 41); ◇, Hvelplund and Andersen (Ref. 42); ◆, Graham *et al.* (Ref. 43); ▲, Goffe, Shah, and Gilbody (Ref. 44); ○, Berkner *et al.* (Ref. 38).

electron-capture cross section from H_2 by protons at low energies. Figure 6 also shows that, as in the case of production of free electrons, the contribution of the autoionizing double capture cannot be neglected at low impact energies and large projectile charges.

Figure 7 shows that our calculations also predict a good dependence of $\sigma_{q,q-1}$ on the projectile charge. This figure also shows that this dependence at low impact energies is not a power of the projectile charge. Only at the highest energy in the figure (200 keV/amu) do the cross sections approximately follow such a law; i.e., $\sigma_{q,q-1}\propto q^{2.4}$. At 500 keV/amu we obtain (not plotted) a behavior $\sigma_{q,q-1}\propto q^{2.9}$, approaching the high-energy behavior $q^{3.15}$ predicted by Schlachter *et al.*[45]

We have devoted Fig. 8 to the analysis of the differences between the capture cross sections from molecular and atomic hydrogen targets for He^{2+} and C^{6+} incident ions. For this purpose, we have plotted in this figure the ratio between the cross sections for these two targets. To calculate our ratio, we have used the CTMC-*r* capture cross sections from atomic hydrogen of Ref. 46, which are in very good agreement with the experimental data for this target. If the hydrogen molecule could be regarded as two free hydrogen atoms, the ratio should be equal to 2 over all the energy range considered. However, Fig. 8 clearly shows that our ratios vary from values smaller than 1 at low impact energies to values as large as 4 at high impact energies. For comparison, we have also included in the figure the empirical scaled ratio predicted by Knudsen, Haugen, and Hvelplund.[19] For C^{6+} projectiles, our ratio is in very good agreement with this scaling law. On the other hand, we disagree, for this incident ion, with the recommended result of Ref. 32 at high impact energies, which predict a ratio that can be as large as 22 at an impact energy of 700 keV/amu. For He^{2+} projectiles, our ratio is in better agreement with the experimental data of Olson *et al.*[39] than with the scaling law of Knudsen, Haugen, and Hvelplund. This departure from the scaling rule for small projectile charges has, however, already been observed by these authors.

In order to get a further insight into the differences between the cross sections for atomic and molecular hydrogen targets, we have included in Fig. 8 the CTMC ratios that are obtained if the capture cross sections from H_2 are assumed to be twice the capture cross sections from a hydrogenlike atom with a binding energy equal to the ionization potential of H_2; i.e.,

$$\sigma_{q,q-1}(H_2)=2\sigma_{q,q-1}[H(E_i=-0.567\text{ a.u.})]\ . \quad (27)$$

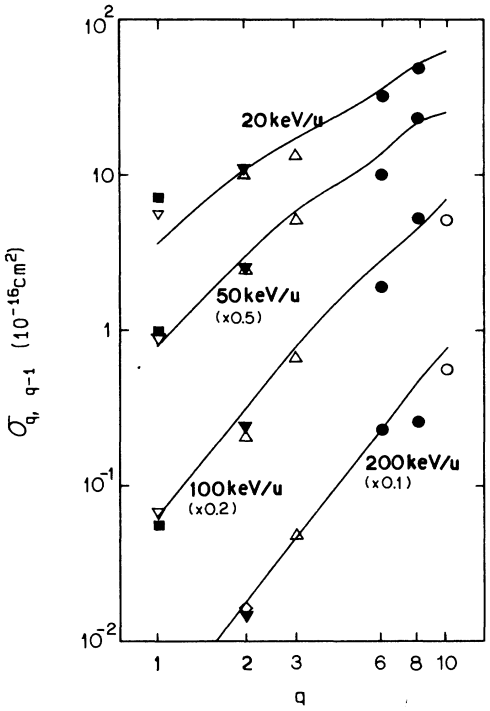

FIG. 7. One-electron capture cross section as a function of the charge state of the impact ion. Solid lines, present work. The symbols are interpolated experimental data from Fig. 6.

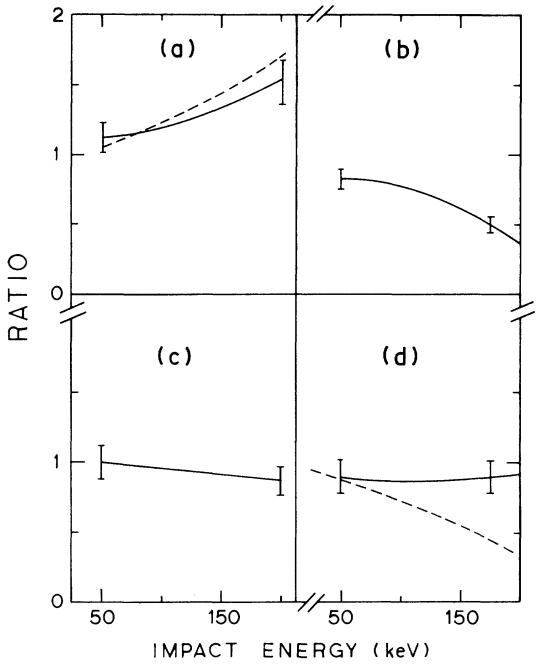

FIG. 9. Ratio of the capture cross sections from H_2 in collision with H^+ for different orientations of the H_2 molecule to that for the randomly orientated molecule. (a) $\mathbf{R}_{H_2}$ parallel to **b**, (b) $\mathbf{R}_{H_2}$ perpendicular to **b** and $\mathbf{v}_p$, (c) $\mathbf{R}_{H_2}$ randomly orientated in a plane perpendicular to $\mathbf{v}_p$, and (d) $\mathbf{R}_{H_2}$ parallel to $\mathbf{v}_p$. Solid lines, present work, with typical standard deviations; dashed lines, Shingal and Lin (Ref. 9).

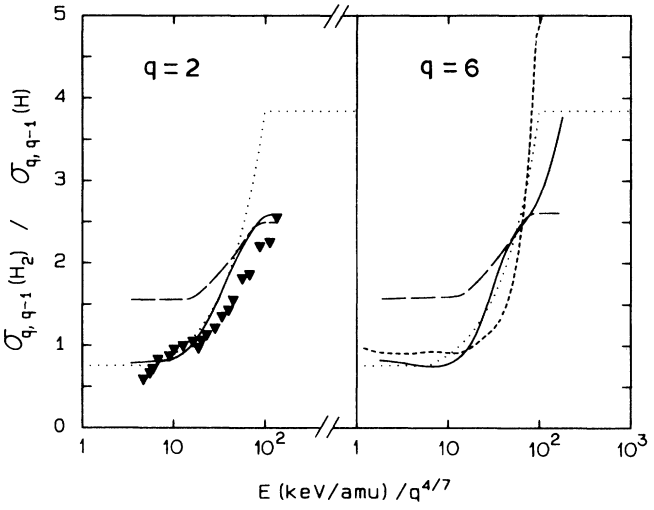

FIG. 8. Ratio between the capture cross sections from H_2 and H targets in collision with He^{2+} and C^{6+} impact ions, as indicated. Solid lines, ratio between present cross sections and CTMC-*r* calculations of Ref. 46, with a standard deviation of 15%. Dotted lines, empirical fitting of Knudsen, Haugen, and Hvelplund (Ref. 19); long-dashed lines, CTMC ratio that is obtained if the capture cross sections from H_2 are approximated by twice the capture cross sections from a hydrogenic atom with an ionization potential equal to 0.567 a.u.; ▽, experimental data of Olson *et al.* (Ref. 39); short-dashed line, empirical prediction of Janev, Phaneuf, and Hunter (Ref. 32).

The ratios that are obtained with this approximation present a behavior similar to the ones discussed above. However, this simple model can only predict the magnitude of the ratio for incident He^{2+} ions at high energies. The same conclusion was obtained by Tuan and Gerjuoy[22] for incident protons and can be easily explained in terms of the differences between the electronic momentum distributions for H and H_2. However, Fig. 8 would indicate that this explanation fails at high energies for incident C^{6+} ions. At low energies, the ratios obtained by means of (27) are about a factor of 2 greater than the actual ones. The large ratio for C^{6+} comes from the fact that the contribution from two-electron processes to the capture cross section is overestimated in this simple scaling. However, this explanation is not applicable for He^{2+} impact. Therefore we believe that the behavior of the ratios at low energies in the He^{2+} case and at high energies in the C^{6+} case could be due to the molecular nature of H_2 (i.e., the two-center nature of this target).

The cross sections presented in the preceding figures were calculated for a randomly oriented H_2 molecule. In Fig. 9 we analyze the dependence of the capture cross section for incident protons on the orientation of the molecule. To this end, we display in this figure the ratio between the cross sections for different orientations and the averaged cross section over a uniformly distributed orientation. Qualitatively, some of the differences between

these ratios can be explained on the basis of the position and momentum distributions of the electrons of the molecule. For example, as the collision energy increases, it is expected that the capture cross section becomes proportional to the probability of finding the electrons around the projectile when it passes through the target. On the other hand, the capture probability is also known to be proportional to the probability that the electrons have an initial velocity similar to that of the impinging ion.

Figures 9(a) and 9(b) show that if the molecule is in the plane perpendicular to the velocity of the projectile, a very different result is obtained when the molecule is either parallel or perpendicular to the impact parameter. This conclusion agrees with the calculations of Shingal and Lin[9] and can be qualitatively understood in terms of the position distribution of the electrons, as discussed above. If the molecule is randomly orientated in the plane perpendicular to the impact velocity [i.e., including the orientations of Figs. 9(a) and 9(b)] a ratio near 1 is obtained [see Fig. 9(c)]. Therefore, in order to observe experimentally the differences between the orientations of Figs. 9(a) and 9(b), it is necessary to measure the angle between the impact parameter and the axis of the molecule.

Figure 9(d) shows that when the molecule is initially orientated in the direction of the impact velocity, our capture cross section is very similar to the averaged cross section. In contrast, the calculations of Shingal and Lin[9] present a very different behavior. This discrepancy may be due to the differences between our momentum distribution and the quantum-mechanical one: While our momentum distribution only depends on the modulus of the momentum, the quantum-mechanical one has an oscillatory dependence on the component of the momentum along the internuclear axis.

IV. SUMMARY

We have successfully developed a classical trajectory Monte Carlo method to study the ionization and electron-capture processes in collisions of multiply charged ions with hydrogen molecules. A very good agreement with the experiments has been obtained in the intermediate impact energy range for a wide variety of charge states of the impact ion. We have found that the autoionizing double capture plays a very important role at low-intermediate energies and charge states of the projectile greater than 2.

We have shown that the differences between the capture cross sections from molecular or atomic hydrogen can only be explained in terms of a two-center model of the H_2 molecule. We have analyzed the contribution of the different orientations of the molecule to the averaged cross section, and we have found that the major contribution comes from the case in which the molecular axis is parallel to the impact parameter.

Further work is in progress on the study of the electron-capture cross sections to the different final electronic states of the projectile by means of the present model. Also, this model will be generalized to include the movement of the heavy particles in the collision dynamics in order to study differential scattering cross sections and their dependence on the orientation of the H_2 molecule.

ACKNOWLEDGMENTS

We would like to thank the Office of Fusion Research of the U.S. Department of Energy for its support and Dr. R. Shingal for providing us with his work prior to publication.

[1]R. Abrines and I. C. Percival, Proc. Phys. Soc. London **88**, 861 (1966).
[2]R. E. Olson and A. Salop, Phys. Rev. A **16**, 531 (1977).
[3]H. Ryufuku, Phys. Rev. A **25**, 720 (1982).
[4]T. G. Winter and L. D. Lin, Phys. Rev. A **29**, 567 (1984).
[5]R. Shakeshaft, Phys. Rev. A **18**, 1930 (1978).
[6]R. E. Olson, T. J. Gay, H. G. Berry, E. B. Hale, and V. D. Irby, Phys. Rev. Lett. **59**, 36 (1987).
[7]C. O. Reinhold and R. E. Olson, Phys. Rev. A **39**, 3861 (1989).
[8]M. Kimura, S. Chapman, and N. R. Lane, Phys. Rev. A **33**, 1619 (1986).
[9]R. Shingal and C. D. Lin, Phys. Rev. A **40**, 1302 (1989).
[10]D. P. Sural and N. C. Sil, J. Chem. Phys. **42**, 729 (1965).
[11]V. Sidis and D. de Bruijn, J. Chem. Phys. **85**, 201 (1984).
[12]C. O. Reinhold and C. A. Falcon, J. Phys. B **21**, 1829 (1988).
[13]R. E. Olson, Phys. Rev. A **18**, 2464 (1982).
[14]G. Peach, S. L. Willis, and M. R. C. McDowell, J. Phys. B **18**, 3921 (1985).
[15]S. L. Willis, G. Peach, and M. R. C. McDowell, J. Phys. B **18**, 3939 (1985).
[16]C. O. Reinhold and C. A. Falcon, Phys. Rev. A **33**, 3859 (1986); (unpublished).
[17]S. J. Pfeifer and R. E. Olson, Phys. Lett. **92A**, 175 (1982).
[18]D. Zajfaman and D. Maor, Phys. Rev. Lett. **56**, 320 (1986).
[19]H. Knudsen, H. K. Haugen, and P. Hvelplund, Phys. Rev. A **24**, 2287 (1981).
[20]M. B. Shah and H. B. Gilbody, J. Phys. B **15**, 3441 (1982).
[21]S. Cheng, E. Y. Kamber, C. L. Cocke, and S. L. Varghese, Nucl. Instrum. Methods **B40/41**, 47 (1989).
[22]T. F. Tuan and E. Gerjuoy, Phys. Rev. **117**, 756 (1960).
[23]M. R. C. McDowell and J. P. Coleman, *Introduction to the Theory of Ion-Atom Collisions* (North-Holland, Amsterdam, 1970), Chap. 4.
[24]J. H. McGuire and L. Weaver, Phys. Rev. A **16**, 41 (1977).
[25]E. McCormack, J. M. Gilligan, C. Cornaggia, and E. E. Eyler, Phys. Rev. A **39**, 2260 (1982).
[26]S. C. Wang, Phys. Rev. A **31**, 579 (1982).
[27]S. Weinbaum, J. Chem. Phys. **1**, 593 (1933).
[28]J. S. Cohen, J. Phys. B **18**, 1759 (1985).
[29]A. E. Wetmore and R. E. Olson, Phys. Rev. A **38**, 5563 (1988).
[30]D. W. Hardie and R. E. Olson, J. Phys. B **16**, 1983 (1983).
[31]R. E. Olson and D. R. Schultz, Phys. Scr. (to be published).
[32]R. K. Janev, R. A. Phaneuf, and H. T. Hunter, At. Data Nucl. Data Tables **40**, 249 (1988).
[33]F. J. de Heer, J. Schutten, and H. Moustafa, Physica **32**, 1766 (1966).
[34]M. E. Rudd, K. D. Dubois, L. H. Toburen, C. A. Ratcliffe, and T. V. Goffe, Phys. Rev. A **28**, 3244 (1983).

[35]M. E. Rudd, T. V. Goffe, and A. Itoh, Phys. Rev. A **32**, 2128 (1985).
[36]L. J. Puckett, G. O. Taylor, and D. W. Martin, Phys. Rev. **178**, 271 (1969).
[37]A. S. Schlachter, K. H. Berkner, W. G. Graham, R. V. Pyle, J. W. Stearns, and J. A. Tanis, Phys. Rev. A **24**, 1110 (1981).
[38]K. H. Berkner, W. G. Graham, R. V. Pyle, A. S. Schlachter, and J. W. Stearns, Phys. Rev. A **23**, 2891 (1981).
[39]R. E. Olson, A. Salop, R. A. Phaneuf, and F. W. Meyer, Phys. Rev. A **16**, 1867 (1977).
[40]M. B. Shah and H. B. Gilbody, J. Phys. B **11**, 121 (1978).
[41]M. B. Shah, T. V. Goffe, and H. B. Gilbody, J. Phys. B **11**, L233 (1978).
[42]P. Hvelplund and A. Andersen, Phys. Scr. **26**, 375 (1982).
[43]W. G. Graham, K. H. Berkner, R. V. Pyle, A. S. Schlachter, J. W. Stearns, and J. A. Tanis, Phys. Rev. A **30**, 722 (1984).
[44]T. V. Goffe, M. B. Shah, and H. B. Gilbody, J. Phys. B **12**, 3763 (1979).
[45]A. S. Schlachter, J. W. Stearns, W. G. Graham, K. H. Berkner, R. V. Pyle, and J. A. Tanis, Phys. Rev. A **27**, 3372 (1983).
[46]C. O. Reinhold and C. A. Falcon, J. Phys. B **21**, 2473 (1988).